AIMS Biophysics

AIMS Biophysics, 13(1): 1−20.
DOI: 10.3934/biophy.2026001
Received: 06 November 2025
Revised: 05 January 2026
Accepted: 08 January 2026
Published: 14 January 2026

http://www.aimspress.com/journal/biophysics

*Research article*

# Dosimetric evaluation of ABS, PLA and NR boluses for electron radiotherapy

**Huda Haddad***

Department of Applied Physics, Tafila Technical University, Tafila, 66110, Jordan

* **Correspondence:** Email: huda.haddad@ttu.edu.jo; Tel: +0096232251346; Fax: +962-3-225-0002.

**Abstract:** *Purpose.* This study aims to compare the dosimetric characteristics of 3D-printed bolus materials acrylonitrile butadiene styrene (ABS), polylactic acid (PLA) with recently introduced natural rubber (NR) bolus. *Materials and Methods*. We employed Monte Carlo simulation to evaluate ABS, PLA, and NR boluses of thicknesses 0.5, 1.0, and 1.5 cm under 6, 9, and 16 MeV electron beam irradiation. Percentage depth dose (PDD) data was analyzed to evaluate dosimetry parameters. Dosimetric stability under varying air-gap conditions was assessed by analyzing PDD curves under air-gap sizes of (0, 1, 3, 5 mm). *Results.* NR and ABS showed similar dosimetric profiles, whereas PLA showed enhanced deeper-tissue protection and provided 0.7–10.2% higher surface dose (SD). PLA also exhibited the highest stability, with SD and $R_{90}$ deviations limited to 1% and 1.2%, respectively, under varying air-gap sizes. At 6 and 9 MeV, a 0.5 cm bolus failed to provide a single dose of 90% of maximum dose for nearly all tested materials *Conclusion.* NR demonstrated comparable dosimetric performance to ABS, serving as a viable substitute. PLA was optimal for maximizing SD and distal tissue sparing while exhibiting the lowest air-gap sensitivity. For tumors located several centimeters deep from the surface, 16 MeV electron beams were suitable. Furthermore, Dual hotspots were identified a substantial risk of localized normal tissue toxicity.

**Keywords:** ABS; bolus; electron bolus; electron radiotherapy; Monte Carlo simulation; natural rubber; PLA

## 1. Introduction

Electron radiotherapy of cancer is widely used as one of the cancer treatment protocols for

superficial regions, accounting for in approximately 90% of cases [1]. Common treatment areas include skin cancers, head and neck cancers, lymphoma, and breast cancer. For example, intraoperative radiotherapy is highly recommended for breast cancer, allowing for the delivery of high-dose radiation directly to the tumor bed immediately after surgical removal [1–4].

High-energy electron beams in the range of 6−20 MeV, as well as photons in the range of 100−250 KVp, are the most effective radiation in fighting superficial tumors [5−7]. Compared to photon beams, electron beams deliver a higher dose to the surface and near-surface region, making them a superior choice for these types of tumors [2].

Optimizing the electron beam by delivering a high dose into the tumor volume and sparing the surrounding tissue is a primary goal in radiotherapy [5−8]. Electron bolus plays a crucial role in achieving this goal for treating superficial tumors. Its clinical functions are to increase the surface dose, compensate for anatomical irregularities to achieve homogeneous dose distribution, and selectively reduce electron penetration in certain areas of the treatment field. Conventional bolus materials, such as paraffin wax and synthetic polymers, are designed with an electron density close to 1 g/cm$^3$ to ensure tissue equivalence [3,9−12]. Supratman et al. demonstrated the potential of natural rubber (NR), composed primarily of cis-polyisopernce, as a promising electron bolus material. Their finding revealed that NR exhibits electron density and mass attenuation coefficients comparable to those of water and soft tissue. These properties, coupled with NR's nontoxicity, ease of fabrication, bubble-free consistency, radiation stability, natural abundance, low cost, and environmental friendliness, align well with the ideal characteristics of bolus materials [13,14].

Several studies have compared the dosimetry characteristics of NR bolus to commercially available alternatives. Aisyah et al. investigated the dosimetry properties of NR bolus in comparison to Poly-Doh and paraffin wax. They concluded that NR can effectively match the dose distribution of clinical boluses, making it a promising substitute [15].

Additionally, Apipunyasopon et al. compared NR to Super flab and TE gel boluses. Their findings suggest that NR is a promising bolus material for radiotherapy due to its density, ease of fabrication, and widespread availability. Moreover, the relative electron density of the NR bolus was very close to that of the Superflab, but different from that of the TE gel. NR demonstrated a more pronounced dose enhancement at the surface compared to TE gel for equivalent thicknesses [13].

Arianto et al. compared NR with silicon rubber (SR) as bolus materials. In their study, Monte Carlo (MC) simulations revealed that the percentage surface dose (PSD) for both NR and SR boluses was nearly identical at 98.4 % and 99.94%, respectively, for a 2 cm bolus thickness [16].

On the other hand, three-dimensional (3D) printing, or additive manufacturing, is an emerging technology that creates structures by building up sequential layers of material. This technology creates samples with high quality and accuracy and gives a solution for some clinical problems such as minimizing the air gap between the bolus and skin to less than 4 mm [8,17−20].

Polylactic acid (PLA) and acrylonitrile butadiene styrene (ABS) are the most widely used materials for 3D printing boluses via fused deposition modelling (FDM). Their well-documented printing parameters and relative ease of use make them popular choices for achieving consistent and reliable print results [2,10−12].

Although 3D-printing technologies, using rigid thermoplastic like ABS and PLA, have emerged as a solution for creating patient- specific boluses, they introduce new challenges. The inherent rigidity of these materials means that any inaccuracy in the 3D-scanning or printing process yields a device that cannot be adjusted during patient setup, potentially leading to persistent air gaps and defeating the

purpose of customization [11].

This study is motivated by the need to fundamentally evaluate how the core material property of elasticity influences bolus performance. We propose a controlled, dosimetric comparison between common rigid 3D-printing polymers (PLA and ABS) and a highly flexible, non-printed benchmark material, NR. Although NR is not a standard 3D-printing filament, it serves as an exemplary model of a traditional, high-conformability bolus material [13,14]. Its intrinsic and extreme flexibility represents one end of the material property spectrum, providing a critical baseline against which to assess the 3D printed rigid, geometrically precise alternatives.

This investigation aims to fill this knowledge gap by employing a systematic MC simulation framework to compare the dosimetric performance of the novel NR bolus with the commonly used 3D-printed PLA and ABS boluses, focusing specifically on dosimetric properties and air gap sensitivity. To complement this**,** a simulated study was conducted. A Solid water phantom covered with these materials with different thicknesses (0.5, 1.0 and 1.5 cm) were irradiated using three megavoltage electron beams (6, 9, and 16 MeV). Percentage depth dose (PDD) data and air gap sensitivity were acquired and analyzed to assess the dosimetry characteristics of each bolus.

## 2. Materials and methods

### *2.1. Study plan*

In this investigation, a solid water phantom was modelled using MC simulation. First, the phantom without a bolus was irradiated with 6, 9, and 16 MeV beams to obtain baseline PDD data. Subsequently, 0.5, 1.0, and 1.5 cm thick bolus layers of the specified materials were added to the phantom. These configurations were irradiated with the same electron beams. PDD data were acquired via MC simulation and visualized in PDD graphs using Origin software. Each graph compares central-axis PDDs for the three bolus materials against the no-bolus reference under identical thickness and energy conditions. To study the effect of air gap size on the stability of dose measurements for the investigated materials, we irradiated 9 MeV beam the bolus- air gap- phantom configuration using four different air-gap sizes (0, 1, 3, and 5 cm). The simulated PDD curves were evaluated by determining the SD and the $R_{90}$ values.

### *2.2. Materials*

Three different bolus materials were investigated: ABS, PLA, and NR. NR was compared to PLA and ABS to evaluate the dosimetric trade-offs between flexible and rigid bolus materials. While PLA and ABS are widely used for patient-specific rigid boluses, their lack of elasticity can lead to air gaps during setup. NR was investigated as a potential alternative offering high conformability. This study aims to determine if NR maintains comparable dosimetric properties (e.g., SD, $R_{90,}$ $R_{80}$ and $R_{50}$) to these standard 3D-printing filaments, alongside a comparative analysis of air gap sensitivity.

Their mass fractions and densities are shown in Table 1. Data for ABS and PLA were generated using ESTAR database of the National Institute of Standards and Technology [21], while data for NR were defined by the International Commission on Radiation Units and Measurements (ICRU Report 44) [22]. To ensure a controlled dosimetric comparison, the simulated boluses (i.e., PLA and ABS) were modeled as solid materials with 100% internal infill. In clinical 3D printing, the density of

a bolus can be intentionally reduced by lowering the infill percentage; however, to maximize bolus effect and minimize internal heterogeneity, 100% infill is generally preferred for radiotherapy applications. The material properties (density and elemental composition) used in the MC environment were adopted from established literature values, as detailed in Table 1, and were not derived from new measurements or calculations.

**Table 1.** Elemental compositions and densities for materials employed in MC simulations.

| Element | PLA [11] mass % | ABS [1] mass % | NR [22] mass % |
|---|---|---|---|
| C | 50 | 84.68 | 88.16 |
| O | 44.46 | - | - |
| H | 5.54 | 7.93 | 11.84 |
| N | - | 7.39 | - |
| Density (g/cm$^3$) | 1.24 | 0.9 | 0.92 |

*2.3. Methods*

2.3.1. MC beam model

In this study, the simulations were conducted by MC simulation using the Electron Gamma Showers (EGSnrc) code toolkit developed by Kawrakow and Rogers [23]. The electron beams employed were selected to have nominal energies of 6, 9, and 16 MeV. Two linear accelerators were simulated using BEAMnrc code [24,25]. Varian Clinac 2100C for 6 and 9 MeV beams and Philips Sl75-20 for 16 MeV beam, the cross-sectional schematics of the simulated accelerator configurations are illustrated in Figure 1. Both units were mimicked through the assigned specifications by manufacturers and by referencing articles demonstrating strong agreement between simulation and experimental data [24−26].

The Philips Sl75-20 machine model was utilized due to the unavailability of a validated 16 MeV IAEA phase-space file for the Varian Clinac 2100C. To ensure that this inconsistency did not confound the results, a sensitivity analysis was conducted at 9 MeV for both models to compare the two source modeling approaches. The results showed that the choice of machine model had a negligible impact on the relative dose distribution and material-specific trends, confirming the robustness of the comparative analysis across different energies.

The field size for all incident electron beams was 10 x 10 cm$^2$ and the source-to-surface distance (SSD) was set to 100 cm. In the Philips Sl75-20 parallel beam of electrons with a 0.1 cm radius was directed along the z-axis at a nominal energy of 16 MeV while phase space (phsp) files obtained from the International Atomic Energy Agency (IAEA) database were used as incident beams for the Varian Clinac 2100C at nominal energies of 6 and 9 MeV [27].

To generate phase-space source files for each simulated beam in both models, 2 x 10$^8$ histories were released. In the EGSnrc parameters, the EXACT and PREST-II algorithms were selected for boundary crossing and electron step, respectively. The variance reduction techniques employed for modeling the irradiation beams are summarized in Table 2.

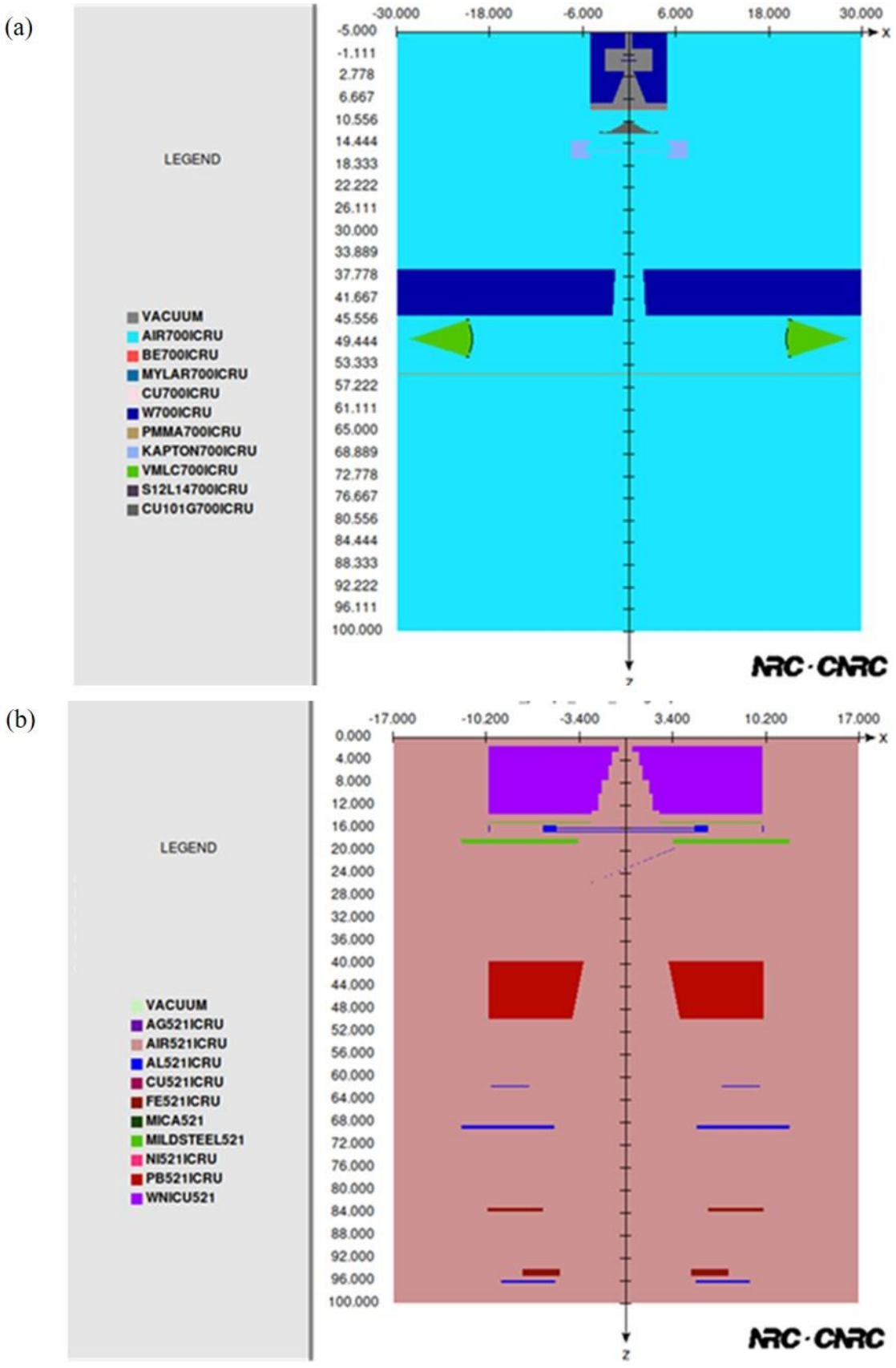


**Figure 1.** Two-dimensional representations of the simulated Linac heads: (a) Varian Clinac 2100C and (b) Philips SL75-20.

The measurements were determined for beam quality according to criteria derived from the IAEA TRS 398 protocol [28]. These specifications included the half-value depth ($R_{50}$), defined as the water depth (in cm) where the dose is half the maximum of the absorbed value, the peak energy in MeV, and the full width of half maximum (FWHM) in MeV. The simulation measurements were performed using Dosxyznrc code [29] and Beamdp [30] and are presented in Table 3.

### 2.3.2. Beam model validation

The MC model was validated by comparing the simulated PDD curves in a water phantom against established benchmarks. For the 6 MeV and 9 MeV beams, the simulations were compared with the IAEA phase-space data for the Varian Clinac 2100C [31]. The validation of 9 MeV is shown in Figure 2. Validation of the 16 MeV beam was conducted by comparing simulated depth-dose parameters with clinical reference values from the IAEA TRS-398 protocol [28]. Key dosimetric parameters showed excellent agreement; specifically, the simulated $R_{50}$ values demonstrated a deviation of less than 0.7% relative to the calculated clinical values. This high level of correspondence across all energy levels confirms the accuracy of the beam modelling.

**Table 2.** The main input parameters in Beamnrc simulation for both model Clinac 2100C and Philips Sl75-20.

| Parameter | Setting/Value | Parameter | Setting/Value |
|---|---|---|---|
| IBRSPL | none | PCUT (MeV) | 0.01 |
| BCSE | off | IREJECT_GlOBAL | On with varying ECUTTER |
| ICM_SPLIT | none | Range Rejection | 2, 4 or 6 * |
| ECUT (MeV) | 0.7 | IFORCE | off |

***** 2, 4, and 6 MeV for 6, 9, and 16 MeV, respectively

**Table 3.** Electron beam specifications for the used radiation.

| Energy (MeV) | Peak (MeV) | FWHM (MeV) | $R_{50}$ (cm) | Unit model |
|---|---|---|---|---|
| 6 | 6.67 | 0.17 | 2.56 | Varian 2100C |
| 9 | 9.23 | 0.30 | 3.70 | Varian 2100C |
| 16 | 14.60 | 0.57 | 5.60 | Philips Sl75-20 |

### 2.3.3. MC phantom specifications

In this investigation, the phantom case study was defined as a 30 x 30 x 30 $cm^3$ solid water cube with voxel size of (0.1 x 0.1 x 0.1 $cm^3$) associated with positional uncertainty margin of (2−3) voxels. The phantom configuration was simulated using Dosxyznrc and analyzed using Statdose code and origin software. The simulation parameters for Dosxyznrc are provided in Table 4.

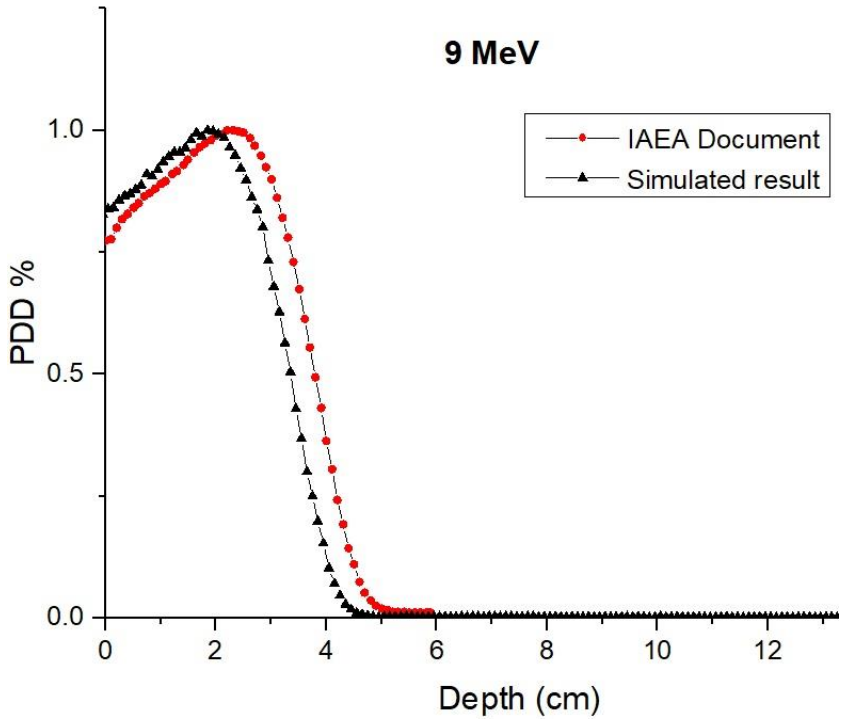


**Figure 2.** Comparison of simulated and reference normalized PDD curves. Reference data obtained from the Varian IAEA phase-space database to validate model accuracy.

**Table 4.** EGSnrc transport parameter used in Dosxyz simulation.

| Parameter | Setting/Value | Parameter | Setting/Value |
|---|---|---|---|
| SMAX | 1e10 | IPCMP | On |
| ESTEPE | 0.25 | comp_xsection | default |
| XImax | 0.5 | IPRDST | Simple |
| Bca_algorithm | Exact | pair_nrc | BH |
| Skindepth_for bca | 0 | IPHTER | Off |
| Transport_algorithm | PRESTA-II | IRAYLR | On |
| Spin_effect | ON | IEDGFL | On |
| Eli_flag | Off | Photon_xsections | xcom |
| IBRDST | Simple | Xsec_out | OFF |
| Brems cross section | BH | | |

To approximate clinical conditions more realistically, an air gap of 0.3 cm was introduced between the bolus and phantom. This gap size was selected due to the widespread use of 3D printing to fabricate boluses, especially for ABS and PLA. This technology typically limits the air gap to less than 0.4 cm. A scheme of simulated configurations with and without bolus is shown in Figure 3.

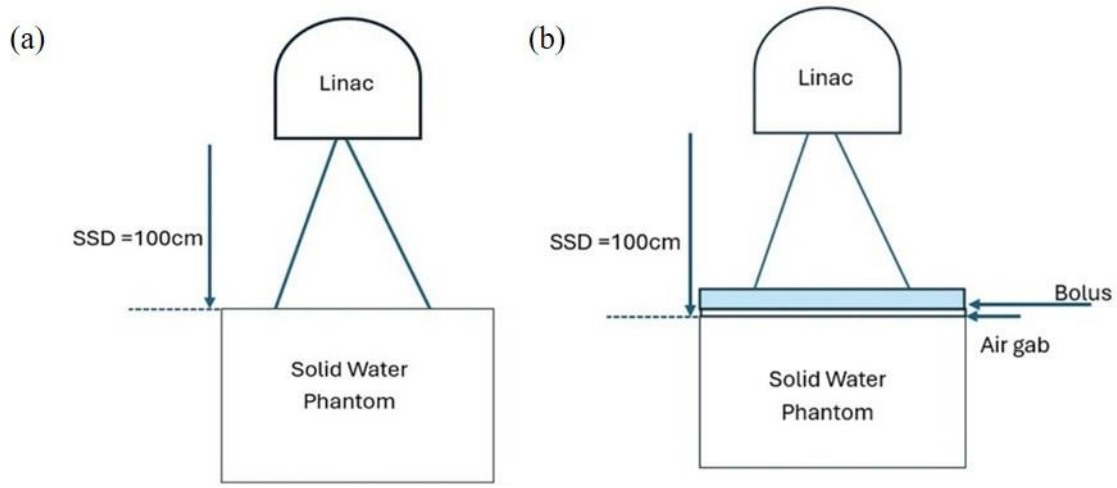


**Figure 3.** A scheme of the simulated model: (a) without bolus, (b) with bolus.

*2.4. Air gap sensitivity*

To quantify the dosimetric sensitivity of the three materials, NR, ABS, and PLA, MC simulations were conducted using a 9 MeV electron beam. The setup involved a 1 cm bolus thick and varying air gaps of 0, 1, 3, and 5 mm. The resulting dose for a comparative assessment of material performance under non-ideal contact conditions distributions were analyzed based in the variations in SD and the depth of the 90% isodose line, allowing for a comparative assessment of material performance under non-ideal contact conditions.

## 3. Results

Figures 4−6 show the PDD curves for the defined phantom under various conditions. Each figure presents the PDDs for the phantom covered with three different bolus materials (ABS, PLA, and NR), as well as for the control phantom (without cover). The PDDs in each figure correspond to the same irradiation energy: 6 MeV (Figure 4), 9 MeV (Figure 5), and 16 MeV (Figure 6). Each material was tested with three bolus thicknesses: 0.5, 1.0, and 1.5 cm.

From the PDD curves obtained for ABS, PLA, and NR boluses, the PSD and key dosimetry parameters were evaluated and are presented in Tables. Table 5 for PSD values followed with Table 6 for a related comparative analysis of PSD. Table 7 for the dosimetric parameters included the depths at 100%, 90%, 80%, and 50% of the maximum dose ($R_{100}$, $R_{90}$, $R_{80}$, and $R_{50}$, respectively). The statistical uncertainty of MC simulation in the present study was lower than 1.5 %, confirming the accuracy and clinical utility of these parameters for quality assurance.

*3.1. Surface dose*

Compared to the no-bolus condition, all bolus configurations resulted in increased surface doses. This increase correlated with increasing bolus thickness. Specifically, as shown in Table 5, PLA demonstrated a higher surface dose than both ABS and NR when boluses of 0.5 cm and 1 cm thickness were used, for all irradiation energies. Table 6 showed an enhancement in the difference in PSD

between PLA and ABS ranged from 0.7% to 10.2% across all investigated energies. Similarly, the difference between PLA and NR showed enhancement ranged from 2.1% to 9.7%.

**Table 5.** The PSD measurements (%) for ABS, PLA and NR across three energy levels (6, 9, and 16 MeV).

| | PSD% | | | | | | | | |
|---|---|---|---|---|---|---|---|---|---|
| Energy (MeV) / Thickness (cm) | ABS | | | PLA | | | NR | | |
| | 6 | 9 | 16 | 6 | 9 | 16 | 6 | 9 | 16 |
| 0.5 | 82.5 | 83.9 | 95.4 | 87.1 | 84.9 | 97.2 | 81.4 | 81.8 | 96.1 |
| 1 | 89.1 | 86.3 | 99.2 | 99.3 | 92.5 | 98.2 | 89.2 | 85.6 | 95.1 |
| 1.5 | 95.8 | 90.9 | 98.6 | 86.3 | 98.6 | 98.2 | 96.9 | 90.5 | 97.9 |

**Table 6.** Comparative analysis of PSD percentage differences between PLA, ABS, and NR for 0.5 and 1 cm thick bolus materials across 6, 9, and 16 MeV electron beams.

| | $\Delta\ (\%) = SD_{PLA} - SD_{ABS}$ | | | $\Delta\ (\%) = SD_{PLA} - SD_{NR}$ | | |
|---|---|---|---|---|---|---|
| Energy (Mev) / Thickness (cm) | 6 | 9 | 16 | 6 | 9 | 16 |
| 0.5 | + 6.1 | + 0.7 | + 1.8 | + 6.3 | + 2.1 | + 2.6 |
| 1 | + 10.2 | + 5.9 | + 2 | + 9.7 | + 6.9 | + 2.5 |

*3.2. Dose profile comparison*

Across all simulated scenarios, a comparison of PDD curves showed a closer dose distribution profiles for ABS and NR, while PLA delivered a lower dose to deeper tissues compared to the other bolus materials under identical conditions. For example, the investigated energies and thicknesses, PLA boluses consistently yielded lower $R_{50}$ and $R_p$ values compared to ABS and NR, e.g., For a 16 MeV beam with a 1 cm bolus, the $R_{50}$ and Rp for PLA were 45.3 mm and 66.6 mm, respectively. In contrast, NR exhibited higher values of 48.7 mm for $R_{50}$ and 68.6 mm for $R_p$, representing a shift in the practical range of 2.0 mm.

**Table 7.** Dosimetry parameters for ABS, PLA, and NR boluses at different thicknesses irradiated by 6, 9 and 16 MeV, the values of R are in (mm).

| 6 MeV | | | | | | |
|---|---|---|---|---|---|---|
| Bolus thickness (cm) | | $R_{100}$ | $R_{90}$ | $R_{80}$ | $R_{50}$ | $R_p$ |
| 0.5 | ABS | 11.0 | 3.54, 15.7 * | 17.4 | 21.3 | 26.3 |
| | PLA | 78.9 | 1.02, 13.7 * | 15.2 | 19.4 | 25.6 |
| | NR | 10.1 | 4.15 | 17.4 | 20.9 | 26.5 |
| 1 | ABS | 5.4 | 6.8, 11.2 * | 13.1 | 16.6 | 22.3 |
| | PLA | 2.11 | 6.47, 15.3* | 8.85 | 13.1 | 19.6 |
| | NR | 6.53 | 0.82,10.6* | 12.7 | 16.5 | 22.1 |
| 1.5 | ABS | 4.15 | 7.10 | 8.98 | 12.5 | 18.4 |
| | PLA | ** | ** | 1.36 | 6.39 | 13.5 |
| | NR | ** | 6.46 | 8.23 | 11.9 | 17.7 |
| 9 MeV | | | | | | |
| | | $R_{100}$ | $R_{90}$ | $R_{80}$ | $R_{50}$ | $R_p$ |
| 0.5 | ABS | 16.8 | 6.87, 25.5 * | 28.6 | 33.6 | 41.4 |
| | PLA | 15.3 | 5.58, 23.7 * | 26.8 | 31.9 | 40.1 |
| | NR | 16.1 | 8.03, 25.5 * | 28.0 | 33.3 | 41.4 |
| 1 | ABS | 12.4 | 3.19, 21.9 * | 24 | 29.3 | 37.2 |
| | PLA | 9.59 | 15.9 | 19.7 | 25.6 | 34.4 |
| | NR | 13.9 | 2.58, 21.1 * | 23.4 | 29.2 | 36.4 |
| 1.5 | ABS | 10.6 | 17.4 | 19.8 | 24.9 | 33.1 |
| | PLA | 2.6 | 9.87 | 12.9 | 19.3 | 27.9 |
| | NR | 10.3 | 16.3 | 19.1 | 24.5 | 31.9 |
| 16 MeV | | | | | | |
| | | $R_{100}$ | $R_{90}$ | $R_{80}$ | $R_{50}$ | $R_p$ |
| 0.5 | ABS | 20.5−25. ☨ | 37.3 | 43.8 | 53.9 | 67.0 |
| | PLA | 9.81−26.7 ☨ | 36.8 | 42 | 51.7 | 65.9 |
| | NR | 5.4−27.4 ☨ | 39.2 | 43.7 | 53.6 | 67.1 |
| 1 | ABS | 14.9−23. ☨ | 35.1 | 40.0 | 49.1 | 62.7 |
| | PLA | 1.8−14.8 ☨ | 30.2 | 35.5 | 45.6 | 59.8 |
| | NR | 10.2−18. ☨ | 33.6 | 38.7 | 49.1 | 62.4 |
| 1.5 | ABS | 5.51−14.1 ☨ | 30.4 | 35.1 | 45 | 58.2 |
| | PLA | 1.52−5.2 ☨ | 22.8 | 27.7 | 38.0 | 54.2 |
| | NR | ** | 27.9 | 33.2 | 44.0 | 58.3 |

*: Dual hot spot **: The values are unavailable in the figure ☨: Represent the Plateau region.

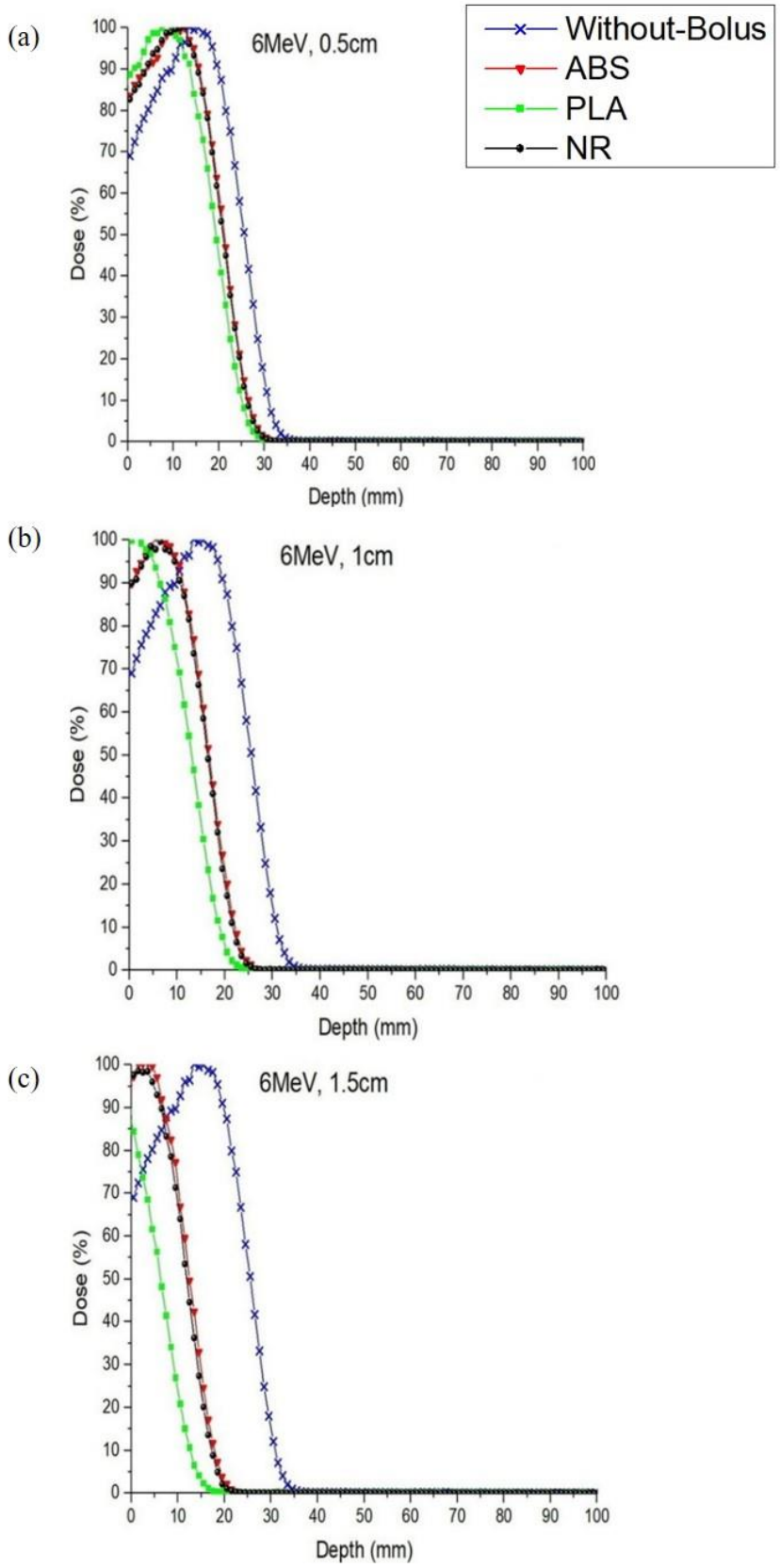


**Figure 4.** PDDs for PLA, ABS, and NR boluses at different thicknesses compared to phantom without bolus exposed to 6 MeV.

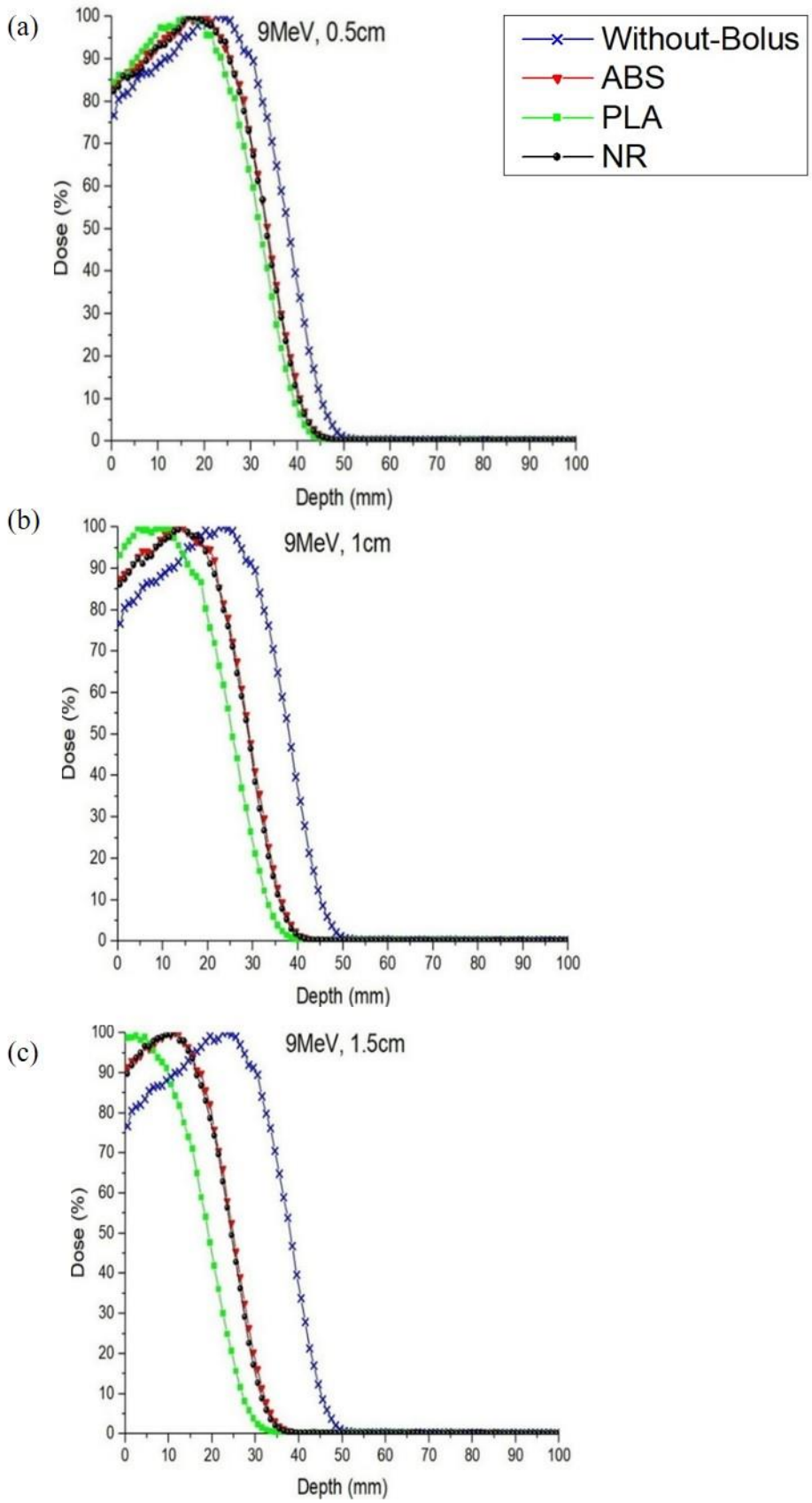


**Figure 5.** PDDs for PLA, ABS, and NR boluses at different thicknesses compared to phantom without bolus exposed to 9 MeV.

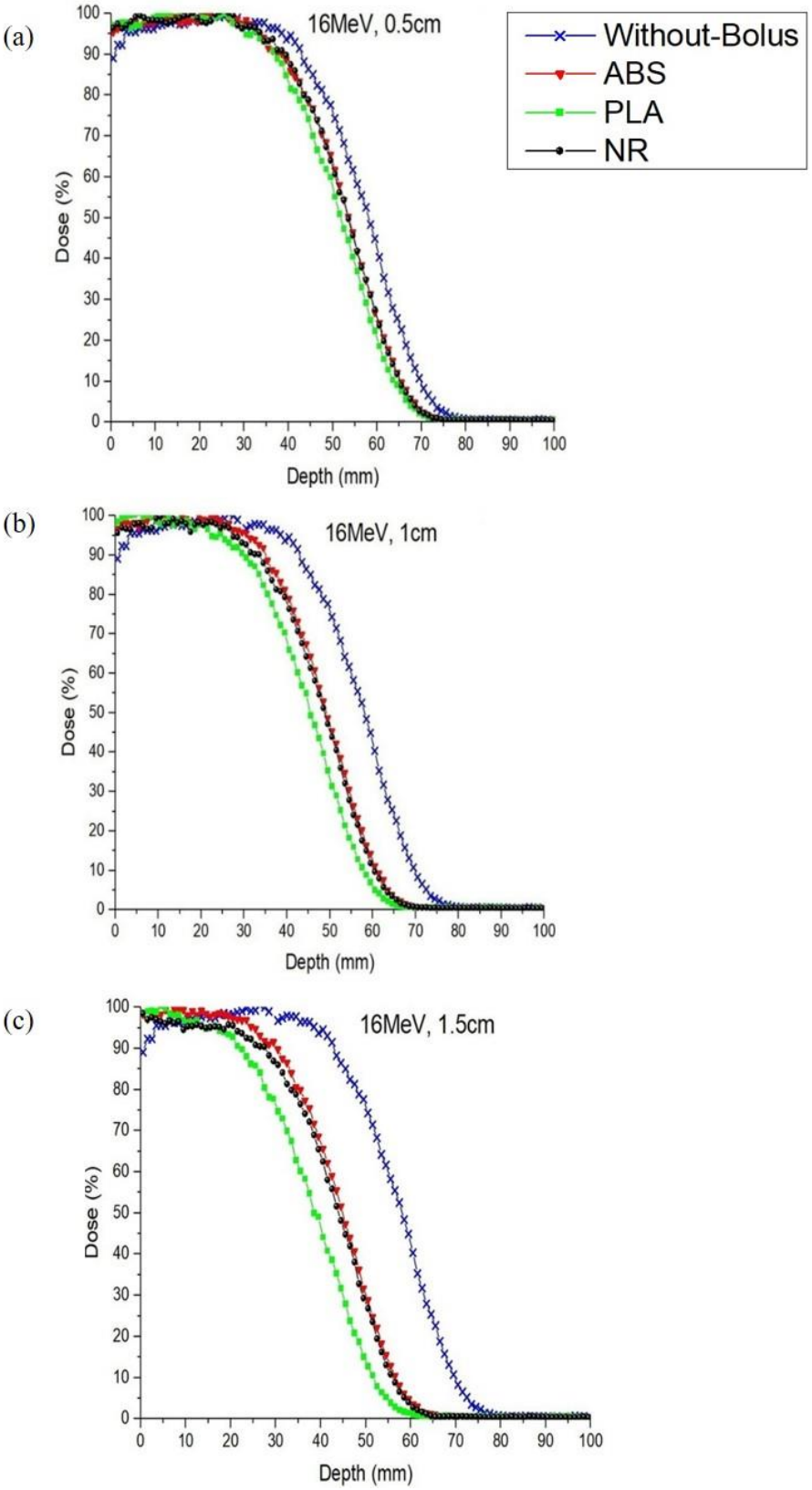


**Figure 6.** PDDs for PLA, ABS and NR boluses at different thicknesses compared to phantoms without bolus exposed to 16 MeV.

*3.3. Dual hotspots*

Table 7 shows dual dose hotspots, e.g. same dose is delivered for two distinct points, at specific parameter combinations. For instance, $R_{90}$ dual hotspots were observed at 6 MeV (0.5 cm bolus, all materials) and 9 MeV (0.5 and 1 cm boluses, all materials). For example, a 9 MeV beam with a 0.5 cm NR bolus, the 90% dose level was achieved at two distinct depths: a proximal point at 8.03 mm and a distal point at 25.5 mm. While with 16 MeV, the location of the $R_{100}$ and $R_{90}$ within the plateau region was difficult to specify a single optimal depth.

*3.4. Plateau region*

At 16 MeV, a characteristic plateau region exists in the dose distribution where the surface dose remains relatively constant over a specific depth. Within this plateau region, the dose profiles for all three bolus materials are nearly identical. The extent of this plateau decreases as bolus thickness increases.

*3.5. Air gap sensitivity*

Table 8 details the dosimetric impact of air gap size on SD and $R_{90}$. Results show that increasing air gaps led to notable variations in SD, whereas the $R_{90}$ depth was minimally affected. The maximum recorded deviations for NR were 2.5% for SD and 0.9% for $R_{90}$. ABS demonstrated slightly higher sensitivity with deviations of 2.6% and 2.3%, while PLA proved the most robust to air gap variations, showing deviations of only 1% and 1.2% for SD and $R_{90}$, respectively.

**Table 8.** Sensitivity analysis of air gap variations on SD and $R_{90}$ for NR, ABS, and PLA bolus at 9 MeV.

| | | NR | | ABS | | PLA | |
|---|---|---|---|---|---|---|---|
| Bolus Thickness (cm) | Air gap (cm) | SD % | $R_{90}$ (cm) | SD (%) | $R_{90}$ (cm) | SD (%) | $R_{90}$ (cm) |
| 1 | 0 | 85.3 | 2.10 | 84.5 | 2.18 | 91.9 | 1.69 |
| | 1 | 87.4 | 2.12 | 85.6 | 2.16 | 92.7 | 1.71 |
| | 3 | 85.6 | 2.11 | 86.7 | 2.18 | 92.5 | 1.61 |
| | 5 | 86.6 | 2.10 | 85.6 | 2.13 | 92.9 | 1.69 |

## 4. Discussion

The results showed that across all energies the reference PDD curves closely matched the expected distribution for an electron beam in tissue-equivalent material, the measured $R_{50}$ was compared to the calculated value from the TRS-398 baseline, the comparison is summarized in Table 3 and illustrated under the "beam model validation" subsection. Adding bolus material to the phantom shifted the PDD curve toward the surface relative to the control phantom curve. This shift toward the surface increased with bolus thickness [3,32]. The analysis of depth-dose distributions reveals distinct trends related to material composition and thickness.

As bolus thickness increases across all materials (ABS, PLA, and NR), a systematic shift in the PDD curves is observed. The thicker bolus provides more material for the electron to interact with before reaching the patient's skin. This interaction leads to increased energy deposition close to the surface, hence a notable shift in the PDD. This shift effectively relocates the build-up region toward the surface, which is a critical requirement for treating superficial lesions while maximizing dose to the skin [32,33].

### *4.1. Surface dose*

The primary observation of "increased surface doses in all cases compared to the no-bolus condition" is a fundamental consequence of using a bolus. The bolus material interacts with the incident electron beam, causing increased energy deposition at or near the surface. The bolus effectively shifts to the build-up region closer to the surface, as mentioned before, hence the increased surface dose.

The finding that "PLA demonstrated a higher surface dose than both ABS and NR" is a more specific and potentially significant observation. This difference in surface dose likely arises from PLA's higher density compared to ABS and NR. Density affects the number of interactions the radiation beam undergoes within the material. A denser material might lead to more interactions and potentially a higher surface dose. Also, different elemental compositions from PLA and NR lead to different interaction cross-sections for radiation. These differences in composition influence the amount of scatter and energy deposition, potentially leading to variations in surface dose [32].

The build-up region's behavior was characterized by a significant thickness-dependent rise in surface dose. For example, Table 5 shows when using an ABS bolus, the transition from 0.5 cm to 1.0 cm thickness increased the surface dose by 6.6% with a comparable increase (6.7%) observed when moving from 1.0 cm to 1.5 cm. This consistent trend demonstrates that for the energies studied, surface dose scales predictably with bolus thickness until the maximus region of dose is reached. Conversely, surface dose enhancement reaches a saturation point as the bolus thickness approaches the $d_{max}$ of the specific electron energy. This phenomenon explains the observed decrease in the surface dose for the 6 MeV beam when using a 1.5 cm PLA bolus (86.3% compared to 99.3 and 87.1 for 1 and 0.5 cm, respectively). In this instance, the surface dose was recorded at 86.3% which is lower than the values obtained for the 0.5 cm and 1.0 cm thicknesses. We conclude that a 1.5 cm bolus exceeds the $d_{max}$ for 6 MeV electrons, effectively placing the measurement point within the distal dose fall-off region rather than the build-up region.

### *4.2. Dose profile comparison*

ABS and NR exhibit similarly when used as boluses. This similarity is likely due to their comparable e, densities and mass attenuation coefficients. The reported densities are 0.9 g/cm$^3$ for ABS and 0.92 g/cm$^3$ for NR as shown in Table 1. While the mass attenuation coefficients are 0.0216 cm$^2$/g for ABS and 0.02216 cm$^2$/g for NR at 9 MeV [34]. The observed disparity in proximal dose gradients, with PLA exhibiting a more pronounced fall-off than NR or ABS, highlights density as a key secondary parameter alongside thickness. This implies for a given thickness, denser materials provide a sharper beam definition in the proximal region. The increased interactions with the incident radiation due to PLA's higher density, resulting in a higher surface dose. Simultaneously, this contributes to a steeper

dose fall-off, delivering a lower dose to deeper tissues and this effect like that of using a thicker bolus. made of ABS or NR.

On the other hand, the dosimetric performance of PLA in this study can be contextualized by comparing it to the work of Kong et al. [3], who investigated the impact of bolus materials, including PLA, glycerol and other materials, on deep-tissue dose deposition. While Kong et al. identified glycerol as the optimal material for distal tissue sparing, their conclusion was likely influenced by the specific physical parameters assigned to their materials. Specifically, they used a lower density for PLA 1.12 g/cm$^3$ compared to glycerol 1.26 g/cm$^3$. In the present study, the PLA was modeled with a higher density of 1.24 g/cm$^3$, which more closely approximates the density of the glycerol used in Kong's research. Furthermore, the elemental composition of our PLA closely mirrors that of glycerol. This suggests that the 'ideal' performance previously attributed to glycerol may be achievable with high-density PLA, effectively bridging the gap between our findings and previous literature. Practically, this enables more precise beam tailoring. By selecting an appropriate PLA thickness, one can simultaneously achieve two clinical objectives: (1) conforming the dose to a specific target depth and (2) more effectively mitigating the skin-sparing effect than is possible with ABS or NR. This positions PLA as a superior material not only for applications, where maximizing normal tissue sparing proximal to the target is critical, but also for delivering a higher dose at the surface.

### *4.3. Dual hotspots*

The observation of "dual hotspots" at specific parameter combinations means that, instead of a single region of high dose, two distinct regions of elevated dose were observed.

These hotspots arise from the interaction of the primary electron beam with the bolus material and the underlying tissue, leading to backscatter that can create localized dose enhancements [35−38].

A 0.5 cm bolus was insufficient to deliver a 90% target dose to a specific location for all materials and energies tested. This was also true for a 1 cm bolus at 9 MeV due to dual dose hotspots. Clinically, dual hotspots pose a significant risk of increased toxicity to healthy tissues, complicating treatment planning by making it more challenging to deliver a homogeneous dose to the tumor volume while sparing surrounding critical structures.

### *4.4. Plateau region*

The energy of the radiation beam affects its penetration depth and the overall dose distribution. Therefore, the impact of the bolus material on surface dose varies with the energy of the incident radiation. In addition to the distance of the treatment device (SSD). Therefore, it is recommended to consider and the accuracy of the treatment plan dose calculation in skin dose assessment [39,40]. However, Lower energy beams deposit their energy more superficially, so the effect of bolus effect is proportionally larger compared to higher energy beams [33]. The energy dependence of the plateau region observed in this study is corroborated by the findings of Diaz Merchan et al. [18]. In their characterization of a novel material (CM) corresponds across an energy range of 6 to 16 MeV, a distinct plateau region emerged at 12 MeV, which became increasingly pronounced at 16 MeV. These observations align with our results, confirming that the plateau region's width is more pronounced at higher energies.

The plateau region in high-energy radiation, which is characterized by a relatively constant

surface dose over a specific depth, offers a valuable clinical advantage for treating tumors extending several centimeters. Positioning the tumor within this region allows for uniform irradiation. Furthermore, the near-identical dose profiles observed for NR, ABS, and PLA boluses at 16 MeV indicate minimal impact of bolus material choice on dose distribution within this plateau region.

### *4.5. Air gap sensitivity*

The results summarized in Table 8 highlight the impact of air gaps on electron scattering and beam degradation. The higher sensitivity of SD, peaking at a 2.6% deviation for ABS, can be attributed to the loss of side-scatter equilibrium when a gap is introduced between the bolus and the phantom. Conversely, the stability of $R_{90}$ indicates that the mean energy of the electron spectrum at depth is less affected by these small air increments than the surface fluence. The divergence between materials is likely linked to their specific electron densities and scattering powers; PLA exhibited the highest level of robustness, maintaining deviations near 1%. These findings suggest that materially divergent bolus options do not respond equally to setup uncertainties, with PLA offering the most predictable dosimetric performance under non-ideal contact conditions. Bolus thickness can be adjusted to control the plateau's extent.

## 5. Conclusions

ABS and NR exhibited remarkably similar radiation responses across all irradiation energies. This suggests that NR could potentially serve as viable and potentially more sustainable for ABS in applications like bolus production for radiation therapy. PLA consistently outperformed both ABS and NR in surface dose delivery across all evaluated energies and thicknesses. With increases of up to 10.2% over ABS and 9.7% over NR, PLA demonstrates a superior capacity for build-up enhancement. Furthermore, the superior stability of PLA (e.g., maintaining deviations within approximately 1% for both surface and deep- tissue metrics) marks it as the most robust material for 3D-printed bolus applications.

The analysis revealed dual $R_{90}$ dose levels at lower energies (6−9 MeV) for thinner boluses (0.5−1 cm), where the 90% isodose line intersected the PDD curve at two separate proximal and distal locations. Additionally, at 16 MeV, a pronounced dose plateau led to spatial ambiguity in defining specific $R_{100}$ and $R_{90}$ positions. These findings highlight potential complexities in characterizing dose distribution for certain energy bolus combinations.

A careful consideration of irradiation energy and bolus thickness is crucial, as certain parameters combinations can lead to undesirable dose hotspots and increased risk of complications.

Future research should focus on further evaluating the biocompatibility, long-term performance of ABS, NR, and PLA boluses to optimize and improve patient outcomes; conducting in-vivo test on patients to see how well these boluses fit irregular body surfaces like the nose and ears; investigating how different printing setting change the density and dose accuracy.

## Use of generative-AI tools declaration

The author declares she has not used Artificial Intelligence (AI) tools in the creation of this article.

## Conflict of interest

The author declares no conflict of interest.

## Author contributions

The author is solely responsible for all aspects of this research, including the study's conception, design, methodology, data acquisition, analysis, interpretation, and the writing of the manuscript.

## References


1. Miloihikova I, Bulavskaya A, Cherepennikov Y, et al. (2019) Feasibility of clinical electron beam formation using polymer materials produced by fused deposition modelling. *Phys Med* 64: 188–194. https://doi.org/10.1016/j.ejmp.2019.07.014
2. Moghaddam SH, Baghani HR, Mahdavi SR (2020) Construction and performance evaluation of a buildup bolus for breast intraoperative electron radiotherapy. *Radiat Phys Chem* 174: 108952. https://doi.org/10.1016/j.radphyschem.2020.108952
3. Kong D, Wu J, Kong X, et al. (2024) Effect of bolus materials on dose deposition in deep tissues during electron beam radiotherapy. *J Radiat Res* 65: 215−222. https://doi.org/10.1093/jrr/rrae001
4. Salguero FJ, Arráns R, Palma BA, et al. (2010) Intensity-and energy-modulated electron radiotherapy by means of an xMLC for head and neck shallow tumors. *Phys Med* 55: 1413. https://doi.org/10.1088/0031-9155/55/5/010
5. Edimo P, Clermont C, Kwato MG, et al. (2009) Evaluation of a commercial VMC++ Monte Carlo based treatment planning system for electron beams using EGSnrc/BEAMnrc simulations and measurements. *Phys Med* 25: 111–121. https://doi.org/10.1016/j.ejmp.2008.07.001
6. Cho S, (2005) Estimation of tumor dose enhancement due to gold nanoparticles during typical radiation treatments: a preliminary Monte Carlo study. *Phys Med Biol* 50: N163–N173. https://doi.org/10.1088/0031-9155/50/15/n01
7. Zheng XJ, Chow JCL (2017) Radiation dose enhancement in skin therapy with nanoparticle addition: A Monte Carlo study on kilovoltage photon and megavoltage electron beams. *World J Radiol* 9: 63–67. http://doi.org/10.4329/wjr.v9.i2.63
8. Wang X, Wang X, Xiang Z, et al. (2021) The clinical application of 3D-printed boluses in superficial tumor radiotherapy. *Front Oncol* 11: 698773. https://doi.org/10.3389/fonc.2021.698773
9. Aldawood FK, Chang SX, Desai S (2020) Design and manufacture of a high precision personalized electron bolus device for radiation therapy. *Med Devices Sens* 3: e10077. https://doi.org/10.1002/mds3.10077
10. Vyas V, Palmer L, Mudge R, et al. (2013) On bolus for megavoltage photon and electron radiation therapy. *Med Dosi* 38: 268–273. https://doi.org/10.1016/j.med dos.2013.02.007
11. Diaz-Merchan JA, Español-Castro C, Martinez-Ovalle SA, et al. (2023) Bolus 3D printing for radiotherapy with conventional PLA, ABS and TPU filaments: theoretical-experimental study. *Appl Radiat Isot* 199: 110908. https://doi.org/10.1016/j.apradiso.2023.110908

12. Cho Y-I, Kim J-H, Bae S-I (2023) Evaluation of shielding performance of tungsten containing 3D printing materials for high-energy electron radiation therapy. *J Korean Soc Radiol* 17: 641–649. https://doi.org/10.1016/j.rpor.2020.06.006
13. Apipunyasopon L, Chaloeiparp C, Wiriyatharaki T, et al. (2020) Characterization of natural rubber as a bolus material for electron beam radiotherapy. *Rep Pract Oncol Radio* 25: 725–729. https://doi.org/10.1088/2053-1591/aad5ca
14. Supratman AS, Sutanto H, Hidayanto E, et al. (2018) Characteristic of natural rubber as bolus material for radiotherapy. *Mater Res Express* 5: 095302. https://doi.org/10.1088/2053-1591/aad5ca
15. Aisyah S, Carina CCC, Nazara T, et al. (2020) A comparative study of dosimetric characterization of bolus based on natural rubber (hevea brasiliensis) and clinical bolus for therapy with megavolt electron radiation. *J Phys Conf* 1505: 012026. 10.1088/1742-6596/1505/1/012026
16. Arianto F, Hidayanto E, Budi WS, et al. (2024) A benchmark for natural rubber (NR) and silicone rubber (SR) as bolus for radiotherapy using Monte Carlo simulation. 12th International seminar on new paradigm and innovation on natural sciences and its applications, 3165: 020004. https://doi.org/10.1063/5.0215893
17. Diaz-Merchan JA, Martinez-Ovalle SA, Vega-Carrillo HR (2023) Development of a 3D printing process of bolus using BolusCM material for radiotherapy with electrons. *Appl Radiat Iso* 1999: 110899. https://doi.org/10.1016/j.apradiso.2023.110899
18. Diaz-Merchan JA, Martinez-Ovalle SA, Vega-Carrillo HR (2022) Characterization of a novel material to be used as bolus in radiotherapy with electrons. *Appl Radiat Isotopes* 183: 110154. https://doi.org/10.1016/j.apradiso.2022.110154
19. Zou W, Fisher T, Zhang M, et al. (2015) Potential of 3D printing technologies for fabrication of electron bolus and proton compensators. *J Appl Clin Med Phys* 16: 90–98. https://doi.org/10.1120/jacmp.v16i3.4959
20. Łukowiak M, Jezierska K, Boehlke M, et al. (2017) Utilization of a 3D printer to fabricate boluses used for electron therapy of skin lesions of the eye canthi. *J Appl Clin Med Phys* 18: 76–81. https://doi.org/10.1002/acm2.12013
21. National Institute of Standard and Technology. Stopping Power and Range Tables for Electrons, Nist. Gov. Available from: https://physics.nist.gov/ PhysRefData/Star/Text/ESTAR.html.
22. Goldstone KE (1989) Tissue Substitutes in Radiation Dosimetry and Measurement in: ICRU Report 44. International Commission on Radiation Units and Measurements, USA.
23. Kawrakow I, Rogers DWO, Mainegra-Hing E, et al. (2000) EGSnrc toolkit for Monte Carlo simulation of ionizing radiation transport. National Research Council of Canada.
24. Rogers DWO, Faddegon BA, Ding GX, et al. (1995) BEAM: a Monte Carlo code to simulate radiotherapy treatment units. *Med Phys* 22: 503–524. https://doi.org/10.1118/1.597552
25. Rogers DWO, Walters B, Kawrakow I (2009) BEAMnrc user's manual, National Research Council Canada. Institute for National Measurement Standards, PIRS-0509 (A) (revL), Ottawa, Canda.
26. Udal MA (1988) Monte Carlo investigation of surface doses for broad electron beams. *Phys Med Biol* 33: 939–953. https://doi.org/10.1088/0031-9155/33/8/004
27. International Atomic Energy Agency, phase-space database for external beam radiotherapy. Available from: https://www-nds.iaea.org/phsp/phsp.htmlx.

28. International Atomic Energy Agency (2000) Absorbed dose determination in external beam radiotherapy: an International Code of Practice for dosimetry based on standards of absorbed dose to water. TRS 398. IAEA, Vienna.
29. Walters B, Kawrakow I, and Rogers DWO (2002) DOSXYZnrc user's manual, National Research Council Report PIRS-794 (revB) Ottawa, Canda.
30. Ma CM, Rogers DWO (1995) BEAMDP user's manual, National Research Council Report PIRS-0509 (C) (revA) Ottawa, Canda.
31. Brualla L, Palanco-Zamora R, Duch MA, et al. (2010) Phase-space files documentation for: Varian Clinac 600 C photon beams and Varian Clinac 2100 C/D electron beams. Institut de Tècniques Energètiques, Universitat Politècnica de Catalunya, Barcelona, Spain.
32. Attix FH (2017) *Introduction to Radiological Physics and Radiation Dosimetry*, 1 Ed., New York: John Wiley and Son, 160−195. https://doi.org/10.1002/9783527617135
33. Khan FM, Gibbons JP (2019) *The Physics of Radiation Therapy*, 6 Eds., Philadelphia: Lippincott Williams & Wilkins, 256–305.
34. Berger MJ, Hubbell JH, Seltzer SM, et al. (2010) XCOM: Photon cross section database.
35. García-Cases F, Perez-Calatayud J, Ballester F, et al. (2018) Peripheral dose around a mobile linac for intraoperative radiotherapy: radiation protection aspects. *J Radiol Prot* 38: 1393. https://doi.org/10.1088/1361-6498/aae5a0
36. Singh S, Semwal MK, Bhatt CP (2019) Estimation of backscatter from internal shielding in electron beam radiotherapy using Monte Carlo simulations (EGSnrc) and Gafchromic film measurements. *J Med Phys* 44: 239-245. https://doi.org/10.4103/jmp.JMP_21_19
37. Fujimoto T, Monzen H, Nakata M, et al. (2014) Dosimetric shield evaluation with tungsten sheet in 4, 6, and 9MeV electron beams. *Phys Med* 30: 838–842. https://doi.org/10.1016/j.ejmp.2014.05.009
38. Chow JCL (2008) Monte Carlo simulation of backscatter from lead for clinical electron beams using EGSnrc. *Med Phys* 35: 1241–1250. https://doi.org/10.1118/1.2874552
39. Demir H, Gul OV, Aksu T (2024) Investigation of skin dose of post-mastectomy radiation therapy for the halcyon and tomotherapy treatment machine: comparison of calculation and in vivo measurements. *Radiat Meas* 1: 107112. https://doi.org/10.1016/j.radmeas.2024.107112
40. Gul OV, Koplay M, Ozturk M (2025) Gantry tilt as a dose reduction strategy for radiosensitive organs in pediatric brain CT: a prospective TLD study. *Radiat Prot Dosim* 202: 8−14. https://doi.org/10.1093/rpd/ncaf144


AIMS Press